ARTICLES
PUBLISHED ONLINE: 8 SEPTEMBER 2013 | DOI: 10.1038/NNANO.2013.176
nature nanotechnology

Current-induced skyrmion dynamics in constricted geometries

Junichi Iwasaki[1]*, Masahito Mochizuki[2] and Naoto Nagaosa[1,3]*

Magnetic skyrmions—vortex-like swirling spin structures with a quantized topological number that are observed in chiral magnets—are appealing for potential applications in spintronics because it is possible to control their motion with ultralow current density. To realize skyrmion-based spintronic devices, it is essential to understand skyrmion motions in confined geometries. Here we show by micromagnetic simulations that the current-induced motion of skyrmions in the presence of geometrical boundaries is very different from that in an infinite plane. In a channel of finite width, transverse confinement results in steady-state characteristics of the skyrmion velocity as a function of current that are similar to those of domain walls in ferromagnets, whereas the transient behaviour depends on the initial distance of the skyrmion from the boundary. Furthermore, we show that a single skyrmion can be created by an electric current in a simple constricted geometry comprising a plate-shaped specimen of suitable size and geometry. These findings could guide the design of skyrmion-based devices in which skyrmions are used as information carriers.

Skyrmions[1], and their crystallization into a triangular lattice, have recently been discovered in some ferromagnets without inversion symmetry (for example, MnSi, $Fe_{1-x}Co_xSi$, Cu_2OSeO_3; refs 2–4) as a consequence of the competition between ferromagnetic exchange coupling J and the Dzyaloshinskii–Moriya (DM) interaction D under an external magnetic field $\mathbf{B}$. In chiral magnets, the ground state for $\mathbf{B} = 0$ is the helical state, which comprises a successive alignment of Bloch domain walls. An increase in B changes the helical phase to the skyrmion-crystal phase at $B = B_{c1}$, and eventually to the ferromagnetic phase at $B = B_{c2}$. The skyrmions have magnetization antiparallel to $\mathbf{B}$ at their centre and parallel to $\mathbf{B}$ at their periphery. Skyrmion crystals are observed experimentally both in bulk samples[2,3] and in thin-plate specimens[5,6].

The energy for each interaction per spin is given by J/ξ^2, D/ξ and B for the ferromagnetic exchange interaction, DM interaction and Zeeman energy, respectively, where ξ is the length scale of the spatial variation of the magnetization. The competition among these three interactions determines the phase diagram and size ξ of the spin texture. The balance between the first two gives $\xi_1 \approx Ja/D$ (where a is the lattice constant and is set to 1 in the following) and the energy scale $E_1 \approx D^2/J = (D/J)^2 J \approx (10^{-2}–10^{-4})J$. Both B_{c1} and B_{c2} are of the order of E_1, and the helix period for $B < B_{c1}$ and the size of the skyrmion for $B_{c1} < B < B_{c2}$ are both of the order of ξ_1. When B is much larger than E_1, however, the balance between the second and third terms determines the length scale as $\xi_2 \approx D/B$. Length scales ξ_1 and ξ_2 are of the order of 3–100 nm, and are much smaller than the size of magnetic bubbles (micrometre scale) induced by the dipolar interaction in thin films of ferromagnets. Note also that the dynamics of magnetic bubbles under current should be identical to that of skyrmions, although the main means for manipulating magnetic bubbles is the magnetic field[7]. Moreover, skyrmions are stable even near room temperature in certain DM magnets[6], and can be manipulated by much lower electric currents than ferromagnetic domain walls[8–10]. These properties—nanometre size, high operational temperature and low threshold current—are advantageous for technical applications relating to high-density storage devices.

To use skyrmions as information carriers we must be able to drive their motion along nanostructures and also nucleate and annihilate them at will. However, knowledge about their motion in constricted geometries is lacking, and generating skyrmions is recognized to be very difficult because of their topological stability; that is, they cannot be created or annihilated by a continuous variation in spin configuration from a uniform ferromagnetic state. This means that a discontinuous flip of the local magnetization is necessary for their creation, which inevitably results in an energy cost of the order of J, although a typical energy scale for a skyrmion per spin is $E_1 \approx (10^{-4}–10^{-2})J$, as defined above. Recently, a method was proposed to create skyrmions using a circulating current[11]. It was also reported that the creation of skyrmions can be achieved with an ultrashort single optical laser pulse[12]. Nucleation of skyrmions from stripe has been also observed in hexaferrite with a Lorentz microscope[13].

In this Article we study the current-induced dynamics of skyrmions in several kinds of constricted geometries using micromagnetic simulation. We find that the confinement and boundary effect drastically change the current-induced skyrmion dynamics, including the steady-state current–velocity relation and transient phenomena, as well as the creation and annihilation of the skyrmions.

Model and simulation

The spin system of chiral magnets is described by a classical Heisenberg model on a two-dimensional square lattice, where the dimensionless local magnetic moments $\mathbf{M_r}$ defined as $\mathbf{M_r} \equiv -\mathbf{S_r}/\hbar$ (where $\mathbf{S_r}$ is the local spin at $\mathbf{r}$ and $\hbar$ is the Planck constant divided by 2π) are treated as classical vectors whose length is fixed as $|\mathbf{M_r}| = M$. We consider the impurity effect by introducing magnetic anisotropy at randomly distributed impurity sites. The Hamiltonian

[1]Department of Applied Physics, The University of Tokyo, 7-3-1, Hongo, Bunkyo-ku, Tokyo 113-8656, Japan, [2]Department of Physics and Mathematics, Aoyama Gakuin University, 5-10-1, Fuchinobe, Sagamihara, 229-8558, Japan, [3]RIKEN Center for Emergent Matter Science (CEMS), Wako, Saitama 351-0198, Japan. *e-mail: nagaosa@riken.jp; iwasaki@appi.t.u-tokyo.ac.jp

is given by

$$\mathcal{H} = -J\sum_{\mathbf{r}}\mathbf{M}_{\mathbf{r}}\cdot\left(\mathbf{M}_{\mathbf{r}+\mathbf{e}_x}+\mathbf{M}_{\mathbf{r}+\mathbf{e}_y}\right) - D\sum_{\mathbf{r}}\left(\mathbf{M}_{\mathbf{r}}\times\mathbf{M}_{\mathbf{r}+\mathbf{e}_x}\cdot\mathbf{e}_x+\mathbf{M}_{\mathbf{r}}\times\mathbf{M}_{\mathbf{r}+\mathbf{e}_y}\cdot\mathbf{e}_y\right) - \mathbf{B}\cdot\sum_{\mathbf{r}}\mathbf{M}_{\mathbf{r}} - A\sum_{\mathbf{r}\in I}\mathrm{M}_{z\mathbf{r}}^2 \quad (1)$$

where $\mathbf{e}_x$ and $\mathbf{e}_y$ are unit vectors for the x- and y-directions respectively, and I denotes a set of positions of impurities. The magnetic field $\mathbf{B}=(0,0,B)$ is applied normal to the plane, and we adopt $J=1$ meV. The typical DM interaction, $D=0.18J$, which is used in most of this Article, gives the transition between the helical and skyrmion-crystal phases at $B_{c1}=0.0075J$, while that between the skyrmion-crystal and ferromagnetic phases is at $B_{c2}=0.0252J$. These values are appropriate for MnSi, as explained in ref. 10. Anisotropy A at the impurity sites is easy-axis along the z-direction when $A>0$ and easy-plane when $A<0$.

We studied the current-induced spin dynamics at $T=0$ by numerically solving the Landau–Lifshitz–Gilbert (LLG) equation (see Methods):

$$\frac{\mathrm{d}\mathbf{M}_{\mathbf{r}}}{\mathrm{d}t} = -\gamma\mathbf{M}_{\mathbf{r}}\times\mathbf{B}_{\mathbf{r}}^{\mathrm{eff}} + \frac{\alpha}{M}\mathbf{M}_{\mathbf{r}}\times\frac{\mathrm{d}\mathbf{M}_{\mathbf{r}}}{\mathrm{d}t} + \frac{pa^3}{2eM}\left(\mathbf{j}(\mathbf{r})\cdot\nabla\right)\mathbf{M}_{\mathbf{r}} - \frac{pa^3\beta}{2eM^2}\left[\mathbf{M}_{\mathbf{r}}\times\left(\mathbf{j}(\mathbf{r})\cdot\nabla\right)\mathbf{M}_{\mathbf{r}}\right] \quad (2)$$

with $\mathbf{B}_{\mathbf{r}}^{\mathrm{eff}} = -(1/\hbar\gamma)(\partial\mathcal{H}/\partial\mathbf{M}_{\mathbf{r}})$. Here, γ is the gyromagnetic ratio, p is the spin polarization of the electric current, and e (>0) is the elementary charge. The second term denotes the Gilbert damping, where α is fixed at $\alpha=0.04$. The third and fourth terms describe the coupling between spins and spin-polarized electric current $\mathbf{j}(\mathbf{r})$. The third term describes coupling via the spin transfer torque and the fourth via non-adiabatic effects. The coefficient of the fourth term, β, determines the strength of the non-adiabatic torque.

The electric current density $\mathbf{j}(\mathbf{r})$ is assumed to be proportional to the electric field $\mathbf{E}(\mathbf{r})=-\nabla\phi(\mathbf{r})$, where $\phi(\mathbf{r})$ is the scalar potential; that is, $\mathbf{j}(\mathbf{r})=\nabla\phi(\mathbf{r})$. Here, the coefficient is absorbed into the definition of $\phi(\mathbf{r})$. For a steady current distribution, the conservation of current, $\nabla\cdot\mathbf{j}=0$, leads to the Poisson equation for $\phi(\mathbf{r})$, $\Delta\phi(\mathbf{r})=0$, which should reflect the system shape with boundary conditions that the current density j is flowing in from the right and flowing out to the left as

$$\frac{\partial\phi}{\partial n} = \begin{cases} j & \text{(at the left end of sample)} \\ -j & \text{(at the right end of sample)} \\ 0 & \text{(otherwise)} \end{cases} \quad (3)$$

See Methods for the numerical method for calculating $\mathbf{j}(\mathbf{r})$.

Skyrmion motion in a finite-width channel

The motion of a skyrmion confined in a narrow region is completely different from that in a non-confined plane because of confining forces from the boundaries. The sample shape considered here is a long stripline-shaped system along the x-direction, with nanometric width w along the y-direction, as shown in the inset of Fig. 1. We set $B=0.0278J$. The relation between the current density j and the drift velocity $v^{(\mathrm{d})}$ of skyrmions in the steady state after the transient time is shown in Fig. 1. Here, the impurity concentration n is fixed at $n=0$ for the clean case and $n=0.1\%$ for the dirty case. Impurity strength A is equal to $0.2J$ (easy-axis anisotropy). For the dirty case we take the average over eight different impurity distributions. Compared with the universal j–$v^{(\mathrm{d})}$ relation of skyrmions without boundary effects[10], the j–$v^{(\mathrm{d})}$ relation in Fig. 1 depends strongly on α, β and the impurity effect, which is very similar to that of the helical phase or ferromagnetic domain walls. When $\beta=0$, in particular, the skyrmion stops even without impurities, which is regarded as intrinsic pinning (Supplementary Movie S1). This characteristic can be explained by the Thiele equation for the centre of mass $\mathbf{R}=(X,Y)$ (refs 14, 15) of a spin texture (see Supplementary Section SI for details):

$$\mathbf{G}\times(\mathbf{v}^{(\mathrm{s})}-\mathbf{v}^{(\mathrm{d})}) + \mathcal{D}(\beta\mathbf{v}^{(\mathrm{s})}-\alpha\mathbf{v}^{(\mathrm{d})}) - \nabla V(\mathbf{r}) = \mathbf{0} \quad (4)$$

where $\mathbf{v}^{(\mathrm{d})}=\dot{\mathbf{R}}$ is the drift velocity of the spin texture and $\mathbf{v}^{(\mathrm{s})}=-(pa^3/2eM)\mathbf{j}$ is the velocity of the conduction electrons, which can be identified as the current density $\mathbf{j}$ besides a factor. The first term in the left-hand side of equation (4) describes the Magnus force with $\mathbf{G}=\mathcal{G}\mathbf{e}_z$ where $\mathbf{e}_z$ is the unit vector along the z-direction and $\mathcal{G}=4\pi Q$ ($Q=-1$ is the skyrmion number) for the skyrmion and $\mathbf{G}=0$ for the domain wall or helix. The second term represents the dissipative force where the components $\mathcal{D}_{ij}$ of the tensor $\mathcal{D}$ are $\mathcal{D}_{xx}=\mathcal{D}_{yy}=\mathcal{D}$ and 0 for otherwise. The third term, $-\nabla V(\mathbf{r})$, stands for the force due to the potential $V(\mathbf{r})$ from the surrounding environment, such as boundaries and impurities. The mechanism for the repulsive potential due to the boundary is that the in-plane tilt at the edge has the opposite direction to that at the perimeter of the skyrmion. We have demonstrated that this mechanism produces the potential barrier in the presence of the DM interaction using a one-dimensional model (Supplementary Section SII).

Let us start with the case of skyrmion motion without a boundary or impurities, that is, $V=0$. In this case, considering the fact that α, $\beta\ll1$ and $\mathcal{D}\approx1$, the dominant term in equation (4) is $\mathbf{G}\times(\mathbf{v}^{(\mathrm{s})}-\mathbf{v}^{(\mathrm{d})})$, so we obtain $\mathbf{v}^{(\mathrm{d})}-\mathbf{v}^{(\mathrm{s})}$, that is, a universal current–velocity relation. The small correction due to α, β gives

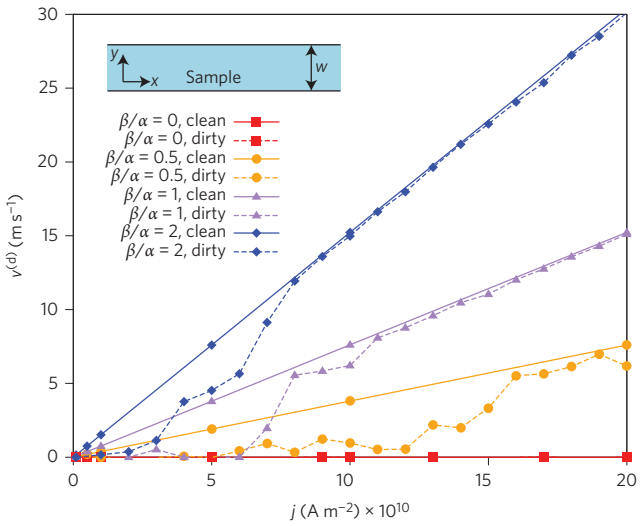

Figure 1 | Steady-state velocity of current-induced motion of a skyrmion after the transient time in a finite-width channel. Drift velocity $v^{(\mathrm{d})}$ of the current-induced steady-state motion of a skyrmion in a finite system as a function of current density j for several values of β/α, where α and β are, respectively, the coefficients of Gilbert damping and the non-adiabatic effect. For the dirty case with an impurity concentration of $n=0.1\%$, values averaged over eight different patterns of impurity distributions are presented. Note that the j–$v^{(\mathrm{d})}$ characteristic for $\beta/\alpha=1$ and $n=0$ is identical to the universal relation for any spin texture at $\alpha=\beta$, which is realized for a skyrmion crystal in a non-confined space even with $\alpha\neq\beta$ (ref. 10). Inset: schematic of a channel of width w.

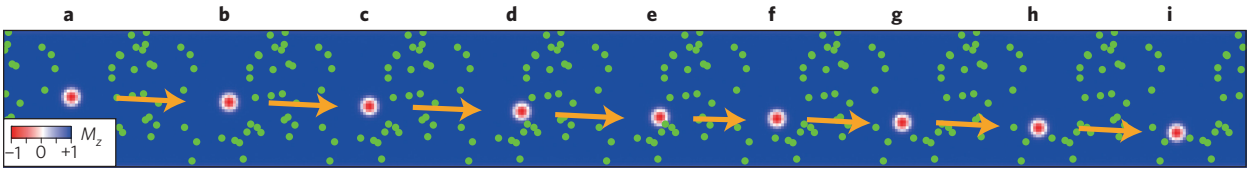

Figure 2 | Transient behaviour of the current-induced motion of a skyrmion in a wide channel. a–i, Snapshots of skyrmion motion in the transient period before it stops beside the boundary in a stripline-shaped system with an impurity concentration of $n = 0.1\%$. The width w of the channel is 150 sites, and the diameter of the skyrmion is ~35 sites. The radius of the skyrmion is defined as twice the distance from the core $M_z = -1$ (red colour) to the perimeter $M_z = 0$ (white colour). The colour plot represents the z-components of the magnetic moments. The numerical simulation is performed for $\beta/\alpha = 0.5$ with current density $j = 5.0 \times 10^{10}$ A m^{-2}, which is below the threshold value in this constricted geometry but well above the critical value in an infinite plane. Positions of the impurities are indicated by green dots. Times corresponding to respective skyrmion positions are $t = 0$ (**a**), $t = 2.08 \times 10^{-8}$ s (**b**), $t = 4.16 \times 10^{-8}$ s (**c**), $t = 6.24 \times 10^{-8}$ s (**d**), $t = 8.32 \times 10^{-8}$ s (**e**), $t = 1.04 \times 10^{-7}$ s (**f**), $t = 1.25 \times 10^{-7}$ s (**g**), $t = 1.46 \times 10^{-7}$ s (**h**) and $t = 1.77 \times 10^{-7}$ s (**i**). The skyrmions are pinned after configuration **i**.

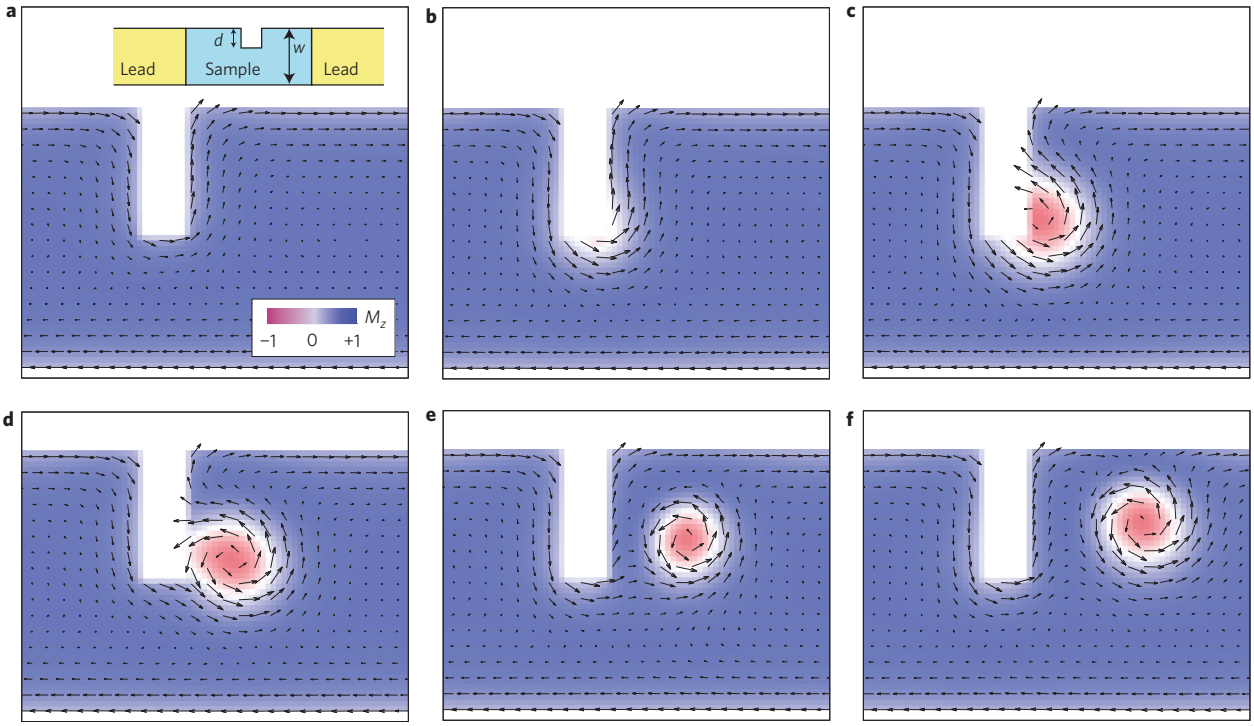

Figure 3 | Creation process for skyrmions. a–f, Snapshots of dynamical spin configurations at selected times in creating a skyrmion for $j = 3.6 \times 10^{11}$ A m^{-2}. In-plane components of the magnetic moments at sites (i_x, i_y) are represented by arrows when $\mathrm{mod}(i_x, 3) = \mathrm{mod}(i_y, 3) = 1$. The colour plot represents the z-components of the magnetic moments. Times corresponding to respective figures are $t = 0$ (**a**), $t = 9.10 \times 10^{-11}$ s (**b**), $t = 18.89 \times 10^{-11}$ s (**c**), $t = 28.60 \times 10^{-11}$ s (**d**), $t = 38.35 \times 10^{-11}$ s (**e**) and $t = 48.10 \times 10^{-11}$ s (**f**). Inset in **a**: schematic of the system with a notch structure for skyrmion creation.

the skyrmion Hall effect transverse to the current given by the additional velocity $\delta\mathbf{v}^{(\mathrm{d})} = \mathbf{e}_z \times \mathcal{D}(\alpha - \beta)\mathbf{v}^{(\mathrm{s})}/\mathcal{G}$. When the pinning force $\mathbf{F}_{\mathrm{pin}} = -\nabla V_{\mathrm{imp}}$ is there, the threshold current density $v_{\mathrm{c}}^{(\mathrm{s})}$ is determined as $v_{\mathrm{c}}^{(\mathrm{s})} \simeq |\mathbf{F}_{\mathrm{pin}}|/|\mathcal{G}|$, which is much smaller than that for domain wall motion where $\mathbf{G} = 0$ and hence $v_{\mathrm{c}}^{(\mathrm{s})} \simeq |\mathbf{F}_{\mathrm{pin}}|/(\beta\mathcal{D})$.

Now we turn to the confined case. In the steady state, the drift velocity $\mathbf{v}^{(\mathrm{d})}$ is along the x-direction while its y-coordinate is non-zero due to the presence of the boundary. In the absence of impurities, V comes from the confining potential and hence $\partial_y V$ is finite near the boundary and $\partial_x V = 0$. Therefore, the x-component of equation (4) reads

$$v_x^{(\mathrm{d})} = \frac{\beta}{\alpha} v_x^{(\mathrm{s})} \tag{5}$$

while that of the y-component

$$\mathcal{G}(v_x^{(\mathrm{s})} - v_x^{(\mathrm{d})}) - \partial_y V = 0 \tag{6}$$

gives the equilibrium condition and determines Y. In other words, the Magnus force is balanced by the confining force, while the dissipative terms determine the velocity. Equation (5) is exactly the same as that for domain wall motion. In the presence of impurities, the threshold current density $v_{\mathrm{c}}^{(\mathrm{s})}$ is determined by $v_{\mathrm{c}}^{(\mathrm{s})} \simeq |\mathbf{F}_{\mathrm{xpin}}|/(\beta\mathcal{D})$, which is again very similar to the case for the domain wall[10]. Assuming the confining potential as $V = Y^2/(2m)$, equation (6) means that Y is the 'momentum' conjugate to X, with m playing the role of mass.

This might appear to be a serious obstacle for applications. However, the distance l a skyrmion travels before it stops can be long (Fig. 2; Supplementary Movies S2 and S3). If the skyrmion starts from the middle of the channel, l reaches more than 0.6 μm for $\beta/\alpha = 0.5$, $j = 5.0 \times 10^{10}$ A m^{-2} ($< j_{\mathrm{c}}^{(\mathrm{pin})}$) and $w = 75$ nm (this value of w is approximately four times larger than the diameter of a skyrmion ($\xi \approx 18$ nm), where the radius is defined as twice the distance from the core $M_z = -1$ to the perimeter $M_z = 0$. The

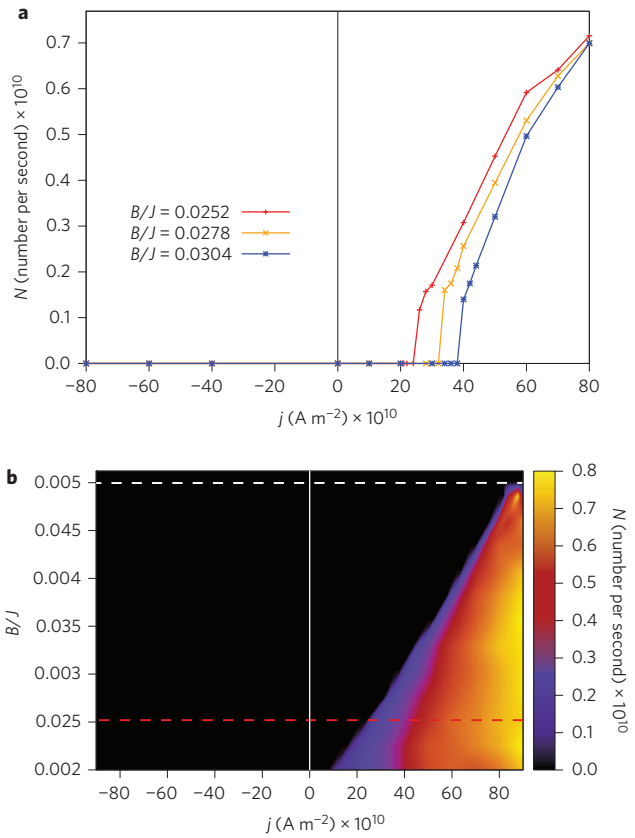

Figure 4 | Rates of skyrmion creation. a, Creation rate N of skyrmions as a function of current density j for several values of magnetic field B. **b**, Colour plot of the creation rate N in the plane of current density j and magnetic field B. The white dashed line indicates the critical magnetic field B_c/J, above which the system cannot hold a metastable skyrmion state. The red dashed line indicates the critical magnetic field B_{c2}/J for the phase transition between skyrmion-crystal and ferromagnetic phases in the ground state. Note that j is positive when the current flows right to left.

distance l could depend on various factors, for example, type or strength of disorder, size of skyrmion, α, β and initial position of the skyrmion. We have investigated other parameter sets and we can conclude that only its initial y-coordinate and $\alpha - \beta$ affect the travelling distance l (Supplementary Section SIII).

Skyrmion nucleation

We next demonstrate the creation of skyrmions in a stripline-shaped system with a square notch structure (Fig. 3, inset). (The notch is often discussed for domain wall pinning[16–18], and the motion of a skyrmion through a triangular notch has been simulated in ref. 19.) Figure 3 presents snapshots of the spin configuration around the notch at selected times when the creation of a skyrmion is observed (Supplementary Movie S4). We fixed the magnetic field at $B = 0.0278J$, which is slightly above B_{c2}. In other words, the ferromagnetic state is the ground state. Spins without electric current have large in-plane components near the boundary due to the DM interaction (Fig. 3a, Supplementary Section SIV). As the electric current flows, the spin texture at the notch swells out due to the spin transfer torque, and one can regard this portion as the seed of a skyrmion (Fig. 3b). Subsequently, spins behind the seed become twisted automatically and point down due to the DM interaction, and eventually the skyrmion core is created (Fig. 3c). This spin twist towards the generation of the skyrmion core is due to spin precession. The unique direction of the precession breaks the reflection symmetry, thereby leading to asymmetry with respect to the sign of j, as shown in the following. At an early stage after its creation, the radius of the created skyrmion oscillates slightly, and eventually the radius converges to arrive at a metastable energy minimum via the Gilbert damping process.

The magnetic structure at the notch, not the winding current pattern, is essential in the creation process. To confirm this, we simulated the dynamics in the following two fictitious conditions. The first condition is a uniform current distribution without modification of the magnetic structure at the notch. In this case, skyrmions are created as in the case of a realistic current distribution. The next condition has a modified magnetic structure such that spins next to the edge are pointed in the z-direction by a huge magnetic field. In this case, skyrmions are never created.

The creation rate of skyrmions N (the number of skyrmions created over time) as a function of current density j for several values of magnetic field B is shown in Fig. 4a. In Fig. 4b, a colour plot of N is presented in the plane of j and B. We find that a larger current density is necessary to create skyrmions under a stronger magnetic field. Surprisingly, skyrmions are created even under a magnetic field that exceeds B_{c2} by a large amount up to B_c, where the skyrmion ceases to be metastable. In addition, the $N - j$ plot is asymmetric between j and $-j$; that is, current flowing in the opposite direction cannot generate skyrmions. The threshold current density $j_c^{(cr)}$ is of the order of $\sim 10^{11}$–10^{12} A m^{-2}. The energy cost to generate a skyrmion is $|(\partial\mathcal{H}/\partial\mathbf{M})| \sim J$, and this energy must be supplied by the electric current. Therefore, the spin transfer torque in the LLG equation should be of the same order as the precession term, namely, $\left|-\gamma\mathbf{M} \times \mathbf{B}^{\mathrm{eff}}\right| \sim \left|(pa^3/2eM)(\mathbf{j} \cdot \nabla)\mathbf{M}\right|$, which leads to

$$j \sim \frac{eJ}{\hbar a^2} \simeq 10^{12}\ \mathrm{A\,m^{-2}} \qquad (7)$$

which is consistent with the obtained $j_c^{(cr)}$.

Creation rate N depends on various conditions. If the depth of the notch, d, is too small (relative to the skyrmion radius), only a portion of a skyrmion can appear inside the sample, so the swirling of spins to create a skyrmion structure cannot be completed, and it eventually disappears as time passes. On the other hand, if d is so large that $w - d$ is small (where w is the sample width), the creation never occurs. The angle of the notch corner, θ, is another issue. We examined five angles, $\theta = 30^\circ$, 45°, 90°, 120° and 135°, and found that 90° is the most suitable for creation. We also studied the case of a rounded notch, and found that skyrmion creation occurs when the curvature radius is comparable to the size of the skyrmion. This means that the sharp edge at the corner of the notch is not essential; it is the in-plane components of the spins along the notch and their shift due to the spin transfer torque that form the essential mechanism. It is noted that a sign change of the DM interaction does not alter the N–j plot (Fig. 4a), whereas that of B exchanges j and $-j$ in Fig. 4a,b.

Skyrmion dynamics at the edge of magnetic material

Finally, we studied the motion at the junction of a magnetic region and non-magnetic leads. The sample considered here is shown in the inset of Fig. 5. We set $B = 0.0278J$ and studied only the clean case ($n = 0$). Two types of skyrmion dynamics near the boundary are presented in Fig. 5. The case with a small current density is shown in Fig. 5a–d (Supplementary Movie S5). The skyrmion bounces and cannot reach the boundary because it cannot overcome a repulsive potential from the boundary. In this bouncing process, the repulsive potential induces a motion transverse to the boundary because of the Magnus force. Eventually, the skyrmion stops at a position slightly below the central line of the system. The larger current density enables a skyrmion to overcome the potential

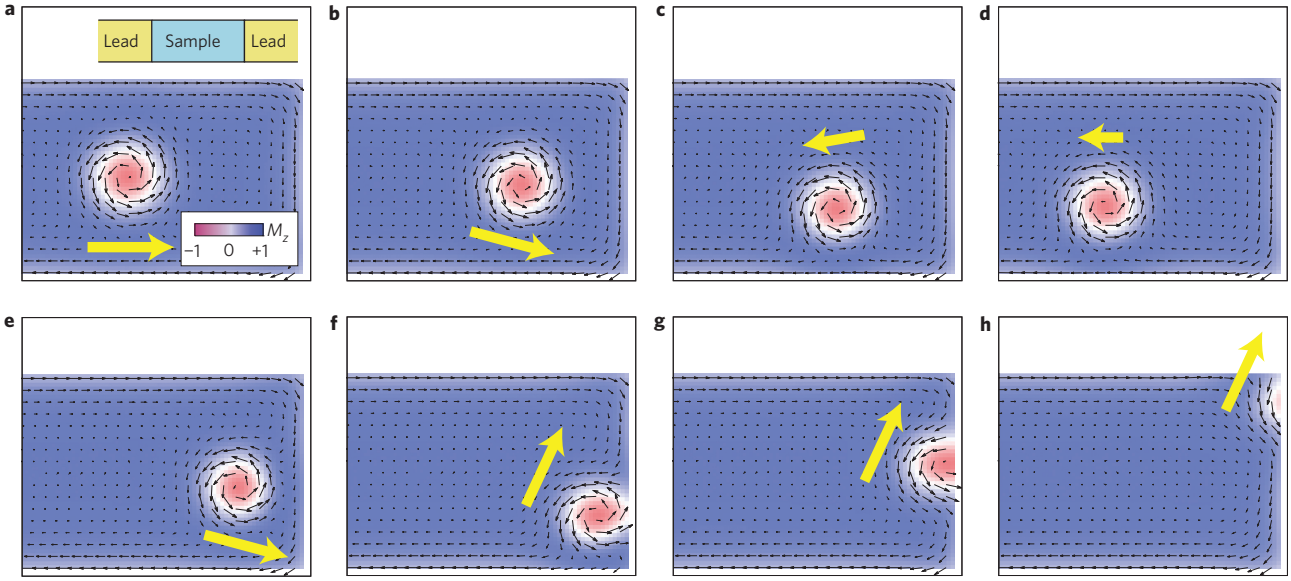

Figure 5 | Two types of skyrmion motion near the edge of the magnetic region. a–h, Snapshots of dynamical spin configurations at selected times near the end of the magnetic region for two different current densities j. In-plane components of the magnetic moments at sites (i_x, i_y) are represented by black arrows when $\mathrm{mod}(i_x, 3) = \mathrm{mod}(i_y, 3) = 1$. The colour plot represents the z-components of the magnetic moments. Yellow arrows indicate the direction and magnitude of velocity at each moment. Current density j is 1.0×10^{11} A m^{-2} for **a–d** and 3.0×10^{11} A m^{-2} for **e–h**. Times corresponding to respective figures are $t = 1.95 \times 10^{-9}$ s (**a**), $t = 2.28 \times 10^{-9}$ s (**b**), $t = 2.60 \times 10^{-9}$ s (**c**), $t = 2.93 \times 10^{-9}$ s (**d**), $t = 8.13 \times 10^{-10}$ s (**e**), $t = 9.10 \times 10^{-10}$ s (**f**), $t = 9.75 \times 10^{-10}$ s (**g**) and $t = 10.08 \times 10^{-10}$ s (**h**). Inset in **a**: schematic of the system with junctions of the magnetic region and non-magnetic leads.

barrier, and pushes the skyrmion to the sample edge, resulting in annihilation of the skyrmion (Fig. 5e–h, Supplementary Movie S6). Because the skyrmion is subject to repulsive and attractive potentials before and after it overcomes the potential barrier, respectively, its trajectory is curved first downward and then upward. The threshold current density $j_c^{(\mathrm{T})}$ between the above two motions is $j_c^{(\mathrm{T})} \simeq 1.5 \times 10^{11}$ A cm^{-2} for $\beta/\alpha = 1$. However, the strength of the boundary barrier can depend on the system parameters. The additional calculations revealed that the size of the skyrmion, which is controlled by the ratio D/B, is the key factor in determining the threshold current density, and a smaller skyrmion can overcome the barrier more easily (Supplementary Section SIII). A detailed analysis based on equation (4) is given in Supplementary Section SI.

Discussion

Some remarks are in order on the magnetic vortex, which has similar dynamics to skyrmions and has been studied intensively[20–24]. Vector $\mathbf{G} = \mathcal{G}\mathbf{e}_z$ in equation (4) for a magnetic vortex is given by $\mathcal{G} = 2\pi pq$ where $p = \pm 1$ specifies the direction of the spin at the centre and $q = \pm 1$ is the vorticity. Although the equation of motion looks similar to the skyrmion case, there are several essential differences. First, the vortex is a non-local object because the spins far away from the centre are winding within the x–y plane, which causes a logarithmic divergence of the energy with respect to the sample size[23]. Therefore, the current-driven motion of a vortex is often studied in a finite-sized sample, for example, of disk shape. This is in sharp contrast to a skyrmion, which has finite size and is regarded as an independent 'particle'. Second, for the magnetic vortex realized in a disk-shaped sample due to the dipolar interaction there are four degenerate states, corresponding to $p = \pm 1$, $q = \pm 1$. It has been demonstrated that p can change during current-driven motion, which results in reversal of the direction of rotational motion[24]. In the case of skyrmions studied in this Article, the stable skyrmion state is unique, with the skyrmion number Q being determined by the direction of the external magnetic field, so its dynamics are stable.

In conclusion, we have found that the j–$v^{(\mathrm{d})}$ relation for a confined skyrmion is similar to that of ferromagnetic domain walls, and have demonstrated a new way to create and annihilate skyrmions in constricted geometries. The creation and annihilation can be controlled easily by an electric current and a magnetic field.

Methods

Numerical simulation of the LLG equation. We used the fourth-order Runge–Kutta method to solve the LLG equation. To study the j–$v^{(\mathrm{d})}$ relation and skyrmion creation, the periodic boundary condition was imposed at the left and right sides of the sample, and the open boundary condition at other boundaries. To study skyrmion annihilation, the open boundary condition was imposed at all boundaries. The natural units of time t and current density j are $\tau \equiv \hbar/J$ and $\kappa \equiv (2eMJ/pa^2\hbar)$, respectively. With a typical lattice constant of $a = 5$ Å, spin-polarization $p = 0.2$ and the magnitude of local magnetic moment $M = 1$, the values of τ and κ become $\tau \simeq 6.5 \times 10^{-13}$ s and $\kappa \simeq 1.0 \times 10^{13}$ A m^{-2}, respectively. We used these values to convert the units of simulated current density and time.

Calculation of current distribution. To solve the Poisson equation $\Delta\phi(\mathbf{r}) = 0$ with the Neumann-type boundary conditions (3), we used the finite-element method[25]. The system was divided into triangular meshes in the following way. We first drew lines between neighbouring sites. In this step, the system was divided into squares of the same size. We then drew a line from the left bottom point to the right top point for each square to complete the triangulation.

Received 25 February 2013; accepted 5 August 2013; published online 8 September 2013; corrected after print 6 January 2014

References

1. Skyrme, T. H. R. A unified field theory of mesons and baryons. *Nucl. Phys.* **31,** 556–569 (1962).
2. Mühlbauer, S. *et al.* Skyrmion lattice in a chiral magnet. *Science* **323,** 915–919 (2009).
3. Münzer, W. *et al.* Skyrmion lattice in the doped semiconductor $Fe_{1-x}Co_x$ Si. *Phys. Rev. B* **81,** 041203(R) (2010).
4. Seki, S., Yu, X. Z., Ishiwata, S. & Tokura, Y. Observation of skyrmions in a multiferroic material. *Science* **336,** 198–201 (2012).
5. Yu, X. Z. *et al.* Real-space observation of a two-dimensional skyrmion crystal. *Nature* **465,** 901–904 (2010).
6. Yu, X. Z. *et al.* Near room-temperature formation of a skyrmion crystal in thin-films of the helimagnet FeGe. *Nature Mater.* **10,** 106–109 (2011).

7. Malozemoff, A. P. & Slonczewski, J. C. in *Magnetic Domain Walls in Bubble Materials* (Academic, 1979).
8. Jonietz, F. *et al.* Spin transfer torques in MnSi at ultralow current densities. *Science* **330,** 1648–1651 (2010).
9. Yu, X. Z. *et al.* Skyrmion flow near room temperature in an ultralow current density. *Nature Commun.* **3,** 988 (2012).
10. Iwasaki, J., Mochizuki, M. & Nagaosa, N. Universal current–velocity relation of skyrmion motion in chiral magnets. *Nature Commun.* **4,** 1463 (2013).
11. Tchoe, Y. & Han, J. H. Skyrmion generation by current. *Phys. Rev. B* **85,** 174416 (2012).
12. Finazzi, M. *et al.* Laser-induced magnetic nanostructures with tunable topological properties. *Phys. Rev. Lett.* **110,** 177205 (2013).
13. Yu, X. Z. *et al.* Magnetic stripes and skyrmions with helicity reversals. *Proc. Natl Acad. Sci. USA* **109,** 8856–8860 (2012).
14. Everschor, K. *et al.* Rotating skyrmion lattices by spin torques and field or temperature gradients. *Phys. Rev. B* **86,** 054432 (2012).
15. Schulz, T. *et al.* Emergent electrodynamics of skyrmions in a chiral magnet. *Nature Phys.* **8,** 301–304 (2012).
16. Kläui, M. *et al.* Direct observation of domain-wall pinning at nanoscale constrictions. *Appl. Phys. Lett.* **87,** 102509 (2005).
17. Martinez, E. *et al.* Thermal effects on domain wall depinning from a single notch. *Phys. Rev. Lett.* **98,** 267202 (2007).
18. Jang, Y. *et al.* Current-induced domain wall nucleation and its pinning characteristics at a notch in a spin-valve nanowire. *Nanotechnology* **20,** 125401 (2009).
19. Fert, A., Cros, V. & Sampaio, J. Skyrmions on the track. *Nature Nanotech.* **8,** 152–156 (2013).
20. Shibata, J. *et al.* Current-induced magnetic vortex motion by spin-transfer torque. *Phys. Rev. B* **73,** 020403 (2006).
21. Guslienko, K. *et al.* Magnetic vortex core dynamics in cylindrical ferromagnetic dots. *Phys. Rev. Lett.* **96,** 067205 (2006).
22. Liu, Y. *et al.* Current-induced magnetic vortex core switching in a permalloy nanodisk. *Appl. Phys. Lett.* **91,** 112501 (2007).
23. Wysin, G. Magnetic vortex mass in two-dimensional easy-plane magnets. *Phys. Rev. B* **54,** 15156–15162 (1996).
24. Yamada, K. *et al.* Electrical switching of the vortex core in a magnetic disk. *Nature Mater.* **6,** 269–273 (2007).
25. Zienkiewicz, O. C., Taylor, R. L. & Zhu, J. Z. in *The Finite Element Method: Its Basis and Fundamentals* (Elsevier Butterworth-Heinemann, 2005).

Acknowledgements

The authors thank Y. Tokura, M. Kawasaki and X.Z. Yu for discussions. This work was supported by Grant-in-Aids for Scientific Research (nos 24224009, 25870169 and 25287088) from the Ministry of Education, Culture, Sports, Science and Technology (MEXT) of Japan, the Strategic International Cooperative Program (Joint Research Type) from Japan Science and Technology Agency and by the Funding Program for World-Leading Innovative R&D on Science and Technology (FIRST Program). M.M. was supported by the G-COE Program 'Physical Sciences Frontier' from MEXT.

Author contributions

J.I. performed the numerical calculations. J.I., M.M. and N.N. contributed to analysing the data and writing the paper.

Additional information

Supplementary information is available in the online version of the paper. Reprints and permissions information is available online at www.nature.com/reprints. Correspondence and requests for materials should be addressed to J.I. and N.N.

Competing financial interests

N.N., M.M. and J.I. have a Japanese patent application for this work, number JPO 2013-045860, 'Creation, annihilation of skyrmion and its application to magnetic devices'.

CORRIGENDUM

Current-induced skyrmion dynamics in constricted geometries

Junichi Iwasaki, Masahito Mochizuki and Naoto Nagaosa

Nature Nanotechnology **8,** 742–747 (2013); published online 8 September 2013; corrected after print 6 January 2014.

In the version of this Article originally published, the authors' competing financial interests were not included. This has now been corrected in the online versions of the Article.